ISSN 0915-633X

NATIONAL INSTITUTE FOR FUSION SCIENCE

Multi-Beamlet Focusing of Intense Negative Ion Beams by Aperture Displacement Technique

Y. Takeiri, O. Kaneko, Y. Oka, K. Tsumori, E. Asano,
R. Akiyama, T. Kawamoto and T. Kuroda

(Received - July 5, 1955)

NIFS-368 Aug. 1995

RESEARCH REPORT
NIFS Series

NAGOYA, JAPAN

Multi-beamlet focusing of intense negative ion beams by aperture displacement technique

Y. Takeiri, O. Kaneko, Y. Oka, K. Tsumori, E. Asano, R. Akiyama,

T. Kawamoto, and T. Kuroda

National Institute for Fusion Science, Nagoya 464-01, Japan

A. Ando

Faculty of Engineering, Tohoku University, Sendai 980-77, Japan

ABSTRACT

Multi-beamlet focusing of an intense negative ion beam has been performed using the beamlet steering by the aperture displacement. The apertures of the grounded grid were displaced as all beamlets of 270 (18 × 15) in the area of 25 cm × 26 cm would be steered to a common point (a focal point) in both the two-stage and the single-stage accelerators. The multi-beamlets were successfully focused and the e-folding half width of 10 cm was achieved 11.2 m downstream from the ion source in both the accelerators. The corresponding gross divergence angle is 9 mrad. The negative ion beamlets are deflected by the magnetic field for the electron deflection at the extraction grid and the deflection direction oppositely changes line by line, resulting in the beam split in the deflection direction. This beamlet deflection was well compensated also using the beamlet steering by the aperture displacement of the grounded grid. The beam acceleration properties related with the beam divergence and the H^- ion current were nearly the same for both the two-stage and the single-stage accelerators, and were dependent on the ratio of the extraction to the acceleration electric fields.

Keywords :

multi-beamlet focusing, negative ion beam, beamlet steering, aperture displacement, high-energy acceleration, beam divergence, negative ion beam transport, negative-ion-based NBI,

I. INTRODUCTION

In the next step fusion experimental devices such as ITER (International Thermonuclear Experimental Reactor), a negative-ion-based neutral beam injection (NBI) system is planned,[1] because the neutralization efficiency of negative ions is as high as 60 % in the high beam-energy range of more than several hundreds keV/N. In order to realize this system much effort has been made to develop high-current and high-energy negative ion sources.[2-16] Recently more than 10 A of negative ion currents have been obtained[12,14,17-19] and high-energy acceleration of more than 100 keV has been demonstrated.[20-22] The negative ion current density is, however, much lower than the positive one, and the grid area of the ion source is larger. As a result, the multi-beamlet focusing by the steering of individual ion beamlets is required for an efficient injection to the torus plasmas.

In the National Institute for Fusion Science, the Large Helical Device (LHD),[23,24] which is the world biggest superconducting helical system, is now under construction, and 125 keV (H)/250 keV (D)-20 MW negative-ion-based NBI is planned for the LHD-plasma heating.[25] For the LHD-NBI system we have developed large negative ion sources,[11,13,15-19,22] and obtained 16.2 A of H^- ion current with the current density of 31 mA/cm^2.[18] We have also achieved a high-energy acceleration of 13.6 A of H^- ion beam to 125 keV.[22] In the LHD-NBI ion source, each grid is divided into grid units of 25 cm × 25 cm in area, which are jointed with a small angle so that all grid units would face a same point. In this structure the multi-beamlets of negative ions delivered from the ion source can be focused at a common point by the beamlet steering in each

grid unit.

Since the negative ion extraction grid contains permanent magnets for the electron suppression, the geometrical shaping of the grid is inapplicable to the multi-beamlet focusing in the negative ion source. On the other hand, the aperture displacement technique for the ion beamlet steering is used for the multi-beamlet focusing in the positive ion sources.[26-30] In the negative ion source, it is reported that using a single negative-ion beamlet, the steering angle of the beamlet by the aperture displacement was measured and agreed with the prediction by the linear optics theory.[31] Therefore, it is important to demonstrate the multi-beamlet focusing of an intense negative-ion beam by the aperture displacement technique.

We have focused the multi-beamlets of negative ions delivered from the grid area of 25 cm × 26 cm on a common point by the aperture displacement of the grounded grid. Moreover, the negative-ion beam deflection by the magnetic field, which is generated by the permanent magnets embedded in the extraction grid, has been compensated also using the beamlet steering by the aperture displacement of the grounded grid. The optimum acceleration conditions of the negative-ion beam focused were investigated for both the two-stage and the single-stage accelerations. In the followings, these results are presented in detail.

II. EXPERIMENTAL SETUP

A. External-filter-type large negative-ion source

In the experiments of the multi-beamlet focusing, an external-filter-type large negative-ion source was used, which has been developed

for the high-energy and high-current negative-ion beam production.[18,22] Figure 1 shows a schematic diagram of the ion source with a two-stage accelerator. The detailed structure is described in refs. 18 and 22. The dimensions of the arc chamber are 30 cm × 62 cm in cross section and 20.6 cm in depth. The ion source is characterized with a strong external magnetic filter produced by a pair of permanent magnet rows with the separation of 35.4 cm. Two cesium ovens are attached to the side wall of arc chamber. In the two-stage acceleration, there are five grids used – plasma grid (PG), extraction grid (EG), electron suppression grid (SG), acceleration grid (AG), and grounded grid (GG), while three grids – PG, EG, and GG, are used in the single-stage acceleration, as shown in Figs. 2 (a) and (b), respectively. Although each grid has 522 (18 × 29) apertures in the area of 25 cm × 50 cm originally, the plasma grid made of molybdenum is masked both upward and downward in the longer direction (Y direction in Fig. 1), resulting in 270 (18 × 15) apertures of 11.3 mm in diameter in the area of 25 cm × 26 cm. The grounded grid has 270 (18 × 15) apertures displaced. As shown in Figs. 2 (a) and (b), the extraction grid contains permanent magnets, which generate the magnetic field suppressing and deflecting the electrons extracted together with the negative ions. In the operation of 522 apertures, this ion source produced 16.2 A of H^- ions, corresponding to 31 mA/cm^2 of the current density at the plasma grid aperture, at the arc efficiency of 0.1 A/kW at the operational gas pressure of 3.8 mTorr in the cesium mode.[18] 13.6 A of H^- ion beam was accelerated to 125 keV in the two-stage acceleration.[22] Thus, the experiments of the multi-beamlet focusing using intense negative ion beams are expected. The operational gas

pressure was around 3.6 mTorr during the experiments in both the two-stage and the single-stage accelerations.

B. Aperture displacement

The steering of ion beamlets by the aperture displacement has been investigated in the positive ion sources,[26-30] and is utilized for the multi-beamlet focusing in the present positive-ion-based NBI system. The theoretical analyses have been performed and compared with the experiments. We have made the apertures of grounded grid displaced, because the steering angle is expected to be proportional to the aperture-displaced amount in both the two-stage and the single-stage accelerations. The negative ion extraction and acceleration systems are shown in Figs. 2 (a) and (b) for the two-stage and the single-stage accelerations, respectively. In both cases, the steering angle, θ, is expressed by

$$\theta = (E_{acc}/4W_B)\ \delta, \tag{1}$$

where δ is the aperture-displaced amount of the grounded grid, E_{acc} the electric field on the upstream side of the grounded grid and W_B the total beam energy.[30] Here, E_{acc} is defined by the applied voltage divided by the grid gap length ($E_{acc} = V_{acc2}/d_{acc2}$ in Fig. 2 (a) and $E_{acc} = V_{acc}/d_{acc}$ in Fig. 2 (b)). Using the focal length of the multi-beamlets, f, and the distance of the aperture position from the grid center, x, the steering angles of the individual beamlets are expressed as $\theta \sim x/f$ for the multi-beamlet focusing and eq. (1) is modified to

$$\delta/x = 4W_B/(E_{acc} f). \tag{2}$$

In the experiments the aperture displacement rates of the grounded grid,

δ / x, were 0.0168 for the two-stage acceleration and 0.0148 for the single-stage acceleration. Although the focal length varies according to the acceleration condition, it ranged 11 to 12 m in the experiments.

On the other hand, the negative ion beam is deflected by the magnetic field generated by the permanent magnets embedded in the extraction grid. As shown in Figs. 2 (a) and (b), the magnetization direction of the permanent magnets is parallel to the beam axis (Z direction in Fig. 1), and the polarity alternately changes line by line along the Y (vertical) direction. The generated field directions on both sides of the extraction grid are opposite to each other, and the magnetic field on the plasma grid side distributes into the arc chamber. Therefore, the line-integrated transverse magnetic field strength along the beam axis is not zero for the negative ion beam, resulting in the beamlet deflection in the X (horizontal) direction. Moreover, the deflection direction in the adjacent beamlets in the Y direction is opposite, because the magnetic field direction alternately changes line by line along the Y direction. Although we will discuss the beam expansion or beam split in the X direction by the alternate horizontal beamlet deflection in section III. A, the beamlet deflection could be compensated by the aperture displacement technique. In the case of the single-stage acceleration, the amount of the aperture displacement of the grounded grid corresponding to the horizontal steering angle of ± 8 mrad is added to that for the multi-beamlet focusing.

C. Negative-ion-based NBI teststand

The ion source is attached to the negative-ion-based NBI teststand[32]

[35] via a gate valve of 800 mm in diameter. The teststand has two large vacuum chambers, the ion source chamber and the beam dump chamber, connected to each other via a 5 m-long neutralizer with the width of 30 cm. During the experiments a cryopump with the pumping speed of 450 m^3/s was operated in the ion source chamber. Two multichannel calorimeter arrays are installed at the entrance and the exit of the neutralizer, and located 5 m and 11.2 m downstream from the ion source, respectively. The calorimeter arrays have 15 channels in the horizontal direction and 25 channels in the vertical direction. The total H^- ion current is estimated using the horizontal and vertical profiles obtained in one shot.

III. EXPERIMENTAL RESULTS

A. Two-stage acceleration

The multi-beamlet focusing in the two-stage acceleration was performed using the grid arrangement shown in Fig. 2 (a). Each aperture of the grounded grid was displaced as each negative ion beamlet would be steered to a focal point, according to eq. (2). However, the beamlet deflection by the magnetic field at the extraction grid is not compensated. The focal length changes by the ratio of the first to the second acceleration electric fields, E_{acc1}/E_{acc2}, in the two-stage acceleration from eq. (2). Therefore, the experimental results presented here were obtained at the constant E_{acc1}/E_{acc2} of around 1, that is equivalent to the single-stage acceleration.

Figures 3 (a) and (b) show the vertical (Y) profiles measured by the calorimeter arrays 5 m and 11.2 m downstream from the ion source,

respectively, and Figs. 3 (c) and (d) show the horizontal (X) profiles measured 5 m and 11.2 m downstream, respectively. The total beam energy is 111 keV, the total H^- ion current detected by the calorimeter array 5 m downstream is 3.8 A, and the second acceleration voltage is 72 kV. The focal length is calculated at 11.8 m on this condition. As shown in Figs. 3 (a) and (b), the vertical profile 5 m downstream is narrow and the vertical profile 11.2 m downstream does not expand, that indicates the gross focusing of the multi-beamlets from the area of 25 cm $\times$ 26 cm. On the other hand, the horizontal profile 5 m downstream is broader, and the horizontal profile 11.2 m downstream is split and the both sides of tails seem to be scraped with the neutralizer wall. Each negative ion beamlet is deflected horizontally by the magnetic field generated at the extraction grid and the deflection direction alternately changes line by line in the vertical direction. As a result, the negative ion beam profile is observed to be split horizontally 11.2 m downstream. We calculated beam profiles using multi-gaussian beamlets of 270 (18 $\times$ 15), each of which has the divergence angle of 9 mrad and the alternate horizontal deflection angle of $\pm$ 8 mrad. The calculated profiles with the focal length of 11.8 m are also indicated by dotted lines in Figs. 3 (a)-(d). The measured profiles are well fitted to the calculated ones both vertically and horizontally at both the calorimeter locations. Thus, the horizontal deflection angle by the magnetic field at the extraction grid is estimated at around 8 mrad at the total beam energy of 111 keV. The gross divergence angle of the negative ion beam is considered at 9 mrad.

The optimum beam acceleration condition, meaning the minimum beam divergence angle with the maximum H^- ion current, was

investigated by varying the ratio of the first acceleration to the extraction electric fields, E_{acc1}/E_{ext}, keeping the E_{acc1}/E_{acc2} constant. Figure 4 (a) shows the FWHMs of the vertical profiles measured 5 m and 11.2 m downstream from the ion source as a function of the E_{acc1}/E_{ext}. The arc power is 70 kW and the extraction voltage is 6.2 kV. The E_{acc1}/E_{acc2} is constant, 0.93, and the focal length is, then, almost constant, around 11.8 m. At around 1.7 of the E_{acc1}/E_{ext}, the FWHMs show the minimums for both the profiles. Although the profile 11.2 m downstream is a little broader than that 5 m downstream, the negative ion beam is not largely broadened vertically during the transport through the neutralizer, because of the multi-beamlet focusing. Figure 4 (b) shows the H^- ion current measured with the calorimeter array 5 m downstream, I_{H^-}, and the ratio of the H^- ion current to the second acceleration current, I_{H^-}/I_{acc2}, as a function of the E_{acc1}/E_{ext}. In contrast with the FWHMs observed in Fig. 4 (a), the I_{H^-} and the I_{H^-}/I_{acc2} show the maximums at around 1.7 of the E_{acc1}/E_{ext}. Since the focal length is 11.8 m in Fig. 4 (a), the e-folding half width of the vertical profile measured 11.2 m downstream is considered to correspond approximately to the gross beam divergence. The e-folding half width of the vertical profile measured 11.2 m downstream is shown in Fig. 5, as a function of the E_{acc1}/E_{ext}, on the same conditions as those in the Fig. 4 (a). The corresponding gross divergence angle estimated from the e-folding half width is also indicated on the right hand axis. The gross divergence angle of 9 mrad is achieved, that is coincident with the results of the profile fitting shown in Fig. 3.

B. Single-stage acceleration

The single-stage acceleration is simpler and more economical than the two-stage acceleration. Since the current density in the negative ion source is much lower than that in the positive ion source, the beam expansion due to the space charge during the acceleration could be lower for the negative ion beam and the single-stage acceleration could be applicable for the high-energy acceleration. From the results in the two-stage acceleration, the optimum beam acceleration was achieved by varying the E_{acc1}/E_{ext} on the condition of the E_{acc1}/E_{acc2} of about 1, that nearly corresponds to the single-stage acceleration. On the other hand, the electron suppression grid is electrically connected to the extraction grid, and, thus, it could be removed. In the experiments in the single-stage acceleration, three-grid system is utilized as shown in Fig. 2 (b). The apertures of the grounded grid are displaced as the individual beamlets would be gathered at a common point and as the alternate horizontal beamlet deflection by the magnetic field at the extraction grid would be compensated. The focal length of the multi-beamlets is chosen at around 11.2 m and the alternate horizontal steering angle to compensate the beamlet deflection by the magnetic field is ± 8 mrad determined from the profile fitting in Fig. 3.

The vertical and horizontal profiles measured 5 m and 11.2 m downstream from the ion source are shown in Figs. 6 (a)-(d). The extraction voltage is 5.2 kV, the acceleration voltage 78 kV and the total H^- ion current estimated with the calorimeter array 5 m downstream 3.8 A. The calculated profiles using multi-gaussian beamlets (18×15) of the focal length of 11.2 m with the divergence angle of 9 mrad and with the alternate horizontal deflection angle of ± 2 mrad are also indicated by

dotted lines in the figures. As shown in Figs. 6 (a)-(d), the profiles are well fitted to the calculated ones. The beam expansion in the horizontal direction by the alternate horizontal beamlet deflection by the magnetic field is not perfectly compensated, and 2 mrad of the alternate deflection seems to exist. However, it is considered that the aperture displacement technique is applicable to the compensation of the alternate beamlet deflection by the magnetic field.

Figure 7 (a) shows the e-folding half width of the vertical profile measured 11.2 m downstream as a function of the acceleration voltage for the extraction voltages of 5.2, 4.3 and 3.4 kV. The arc power is 60 kW. The divergence angle corresponding to the e-folding half width is also indicated on the right hand axis in the figure. The acceleration voltage giving the minimum divergence becomes higher as the extraction voltage is higher. Figure 7 (b) shows the total H^- ion current measured 11.2 m downstream, which passes through the neutralizer, as a function of the acceleration voltage for the same extraction voltages as those in Fig. 7 (a). Although the acceleration voltage giving the maximum H^- ion current becomes higher as the extraction voltage is higher, the maximum H^- ion current for a fixed extraction voltage increases as the extraction voltage increases. This is because the extraction voltages of 4.3 and 3.4 kV are too low to extract fully the negative ions produced at the arc power of 60 kW. As shown in Figs. 7 (a) and (b), the acceleration voltage giving the minimum divergence is a little higher than that giving the maximum H^- ion current.

The ratio of the acceleration to the extraction electric fields, E_{acc}/E_{ext}, has an influence on the beam properties. Figures 8 (a) and (b)

show the e-folding half width of the vertical profile and the total H^- ion current measured 11.2 m downstream, respectively, as a function of the E_{acc}/E_{ext}. The arc powers are 60 kW for the extraction voltages of 5.2, 4.3 and 3.4 kV and 35 kW for the extraction voltages of 4.4 and 3.6 kV. The corresponding divergence angle is also indicated on the right hand axis in Fig. 8 (a). It is recognized that the dependency of the e-folding half width on the E_{acc}/E_{ext} is nearly the same for the various combinations of the extraction voltage and the arc power, as well as that of the H^- ion current. The minimum divergence angles are nearly the same for the different arc powers, at which the negative ion currents are different. Although the E_{acc}/E_{ext} giving the minimum divergence is a little higher than that giving the maximum H^- ion current, these dependencies on the E_{acc}/E_{ext} are relatively broad. Thus, in the single-stage acceleration the ion source should be operated on the condition for the maximum H^- ion current due to the high acceleration efficiency.

Although the electron suppression grid is removed in the single-stage acceleration, no increase of the current ratio of the acceleration current to the H^- ion current, I_{acc}/I_{H^-}, i.e., no increase of the accelerated electron current, was observed.

IV. DISCUSSIONS

The multi-beamlets of the negative ion beam are successfully focused by the aperture displacement technique. In both the two-stage and the single-stage accelerations the aperture displacement of the grounded grid is effective for the beamlet steering, because a linear correlation between the amount of the displacement and the steering

angle is simple as indicated in eq. (1) and the steering angle is not largely dependent on the total beam energy. The alternate horizontal deflection of the negative ion beamlets by the magnetic field at the extraction grid is compensated also by the aperture displacement technique. The line-integrated transverse magnetic field strength generated by the embedded permanent magnets in the extraction grid, $\int$ Bdz, is 200-300 G cm along the beam axis depending on the negative ion emitting surface. The corresponding beamlet deflection angle, θ_m, is approximately estimated at 4-7 mrad at the beam energy of 100 keV from a simple equation,

$$\theta_m = \sqrt{e/2MV} \int Bdz \quad , \tag{3}$$

where M is the ion mass, V the total acceleration voltage and e the electron charge. The deflection angle determined by the profile fitting in Figs. 3 (a)-(d) is 8 mrad, suggesting that the negative ion emitting surface could be extruded toward the extraction grid. The detailed experiments using a single beamlet are required for the relation between the deflection angle and the emitting surface position. In the case of the single-stage acceleration, the aperture displacement for the alternate beamlet steering angle of $\pm$8 mrad is added to that for the multi-beamlet focusing. As shown in Figs. 6 (a)-(d), the deflection angle of 2 mrad is not compensated, because the total beam energy in Fig. 6 is lower than that in Fig. 3. The deflection angle by the magnetic field is dependent on the square root of the total energy, and the deflection angle in Fig. 6 is calculated to be larger by about 1.2 mrad than that in Fig. 3. Therefore, the beamlet deflection by the magnetic field is considered to be well

compensated by the aperture displacement technique. However, it is noted that the beamlet steering angle by the aperture displacement is independent of the beam energy while the beamlet deflection angle by the magnetic field is dependent on it. In an actual injector, the beam energy is varied less than 40 %, and the deflection angle changes by 1-2 mrad at most. The accuracy of the amount of aperture displacement also has an influence on the steering angle. In the case of the single-stage acceleration shown in Fig. 2 (b), the steering angle changes by 0.6 mrad when the amount of the displacement deviates by 0.1 mm. The deviation of the displacement amount is caused by the fabrication accuracy and the thermal expansion of the grid, and the changes of individual steering angle result in the aberration of the multi-beamlet focusing. However, since the displacement accuracy of 0.1 mm is possibly achieved, this aberration would hardly cause serious problems.

In conclusion the multi-beamlet focusing of an intense negative ion beam is achieved with the gross divergence angle of 9 mrad by the aperture displacement technique, and the beamlet deflection by the magnetic field generated at the extraction grid is compensated also by it. These results enable to transport the intense negative ion beam to a long distance.

REFERENCES

1 T. Nagashima, R. S. Hemsworth, M. Makowski, D. Remsen, and the ITER Joint Central Team and Home Teams, *Proc. of the 15th Int. Conf. on Plasma Physics and Controlled Nuclear Fusion Research, Seville, Spain, 1994*, IAEA-CN-60/E-P-9.

2 M. Bacal, G. W. Hamilton, A. M. Bruneteau, H. J. Doucet and J. Taillet, Rev. Sci. Instrum. **50**, 719 (1979).

3 K. N. Leung, K. W. Ehlers and M. Bacal, Rev. Sci. Instrum. **54**, 56 (1983).

4 R. L. York, Ralph R. Stevens, Jr., K. N. Leung and K. W. Ehlers, Rev. Sci. Instrum. **55**, 681 (1984).

5 M. Bacal, A. H. Bruneteau and M. Nachman, J. Apple. Phys. **55**, 15 (1984).

6 A. J. T. Holmes, G. Dammerts and T. S. Green, Rev. Sci. Instrum. 56, 1697 (1985).

7 Y. Okumura, H. Horiike, T. Inoue, T. Kurashima, S. Matsuda, Y. Ohara and S. Tanaka, *Proc. of the 4th Int. Symp. on Production and Neutralization of Negative Ions and Beams, Upton, NY, 1986*, AIP Conf. Proc. No. 158, p. 309.

8 A. J. T. Holmes, L. M. Lea, A. F. Newman and M. P. S. Nightingale, Rev. Sci. Instrum. **58**, 223 (1987).

9 K. N. Leung, K. W. Ehlers, C. A. Hauck, W. B. Kunkel and A. F. Lietzke, Rev. Sci. Instrum. **59**, 453 (1988).

10 M. Hanada, T. Inoue, H. Kojima, Y. Matsuda, Y. Ohara, Y. Okumura, K. Watanabe and M. Seki, Rev. Sci. Instrum. **61**, 499 (1990).

11 Y. Takeiri, A. Ando, O. Kaneko, Y. Oka, R. Akiyama, T. Kawamoto, A.

Karita, K. Mineo and T. Kuroda, *Proc. of the 16th Symp. on Fusion Technology, London, 1990*, p. 1012.

12 Y. Okumura, M. Hanada, T. Inoue, H. Kojima, Y. Matsuda, Y. Ohara, Y. Oohara, M. Seki, Y. Suzuki and K. Watanabe, *Proc. of the 16th Symp. on Fusion Technology, London, 1990*, p. 1026.

13 A. Ando, Y. Takeiri, K. Tsumori, O. Kaneko, Y. Oka, R. Akiyama, T. Kawamoto, K. Mineo, T. Kurata and T. Kuroda, Rev. Sci. Instrum. **63**, 2683 (1992).

14 Y. Okumura, M. Hanada, T. Inoue, H. Kojima, Y. Matsuda, Y. Ohara, M. Seki and K. Watanabe, *Proc. of the 5th Int. Symp. on the Production and Neutralization of Negative Ions and Beams, Brookhaven, 1990*, AIP Conf. Proc. No. 210, p. 169.

15 A. Ando, K. Tsumori, Y. Takeiri, O. Kaneko, Y. Oka, T. Okumura, H. Kojima, Y. Yamashita, R. Akiyama, T. Kawamoto, K. Mineo, T. Kurata and T. Kuroda, *Proc. of the 6th Int. Symp. on Production and Neutralization of Negative Ions and Beams, Upton, NY, 1992*, AIP Conf. Proc. No. 287, p. 339.

16 K. Tsumori, A. Ando, Y. Takeiri, O. Kaneko, Y. Oka, T. Okuyama, H. Kojima, Y. Yamashita, T. Kawamoto, R. Akiyama and T. Kuroda, Rev. Sci. Instrum. **65**, 1195 (1994).

17 A. Ando, K. Tsumori, Y. Oka, O. Kaneko, Y. Takeiri, E. Asano, T. Kawamoto, R. Akiyama and T. Kuroda, Phys. Plasmas **1**, 2813 (1994).

18 Y. Takeiri, A. Ando, O. Kaneko, Y. Oka, K. Tsumori, R. Akiyama, E. Asano, T. Kawamoto, T. Kuroda, M. Tanaka and H. Kawakami, Rev. Sci. Instrum. **66**, 2541 (1995).

19 Y. Takeiri, A. Ando, O. Kaneko, Y. Oka, K. Tsumori, T. Takanashi, R.

Akiyama, E. Asano, T. Kawamoto, M. Tanaka, H. Kawakami, T. Okuyama, Y. Suzuki and T. Kuroda, *Proc. of the 18th Symposium on Fusion Technology, Karlsruher, 1994*, to be published.

20 J. Pamela, M. Fumelli, F. Jequier, A. Simonin, M. Hanada, Y. Okumura and K. Watanabe, *Proc. of the 6th Int. Symp. on Production and Neutralization of Negative Ions and Beams, Upton, NY, 1992*, AIP Conf. Proc. No. 287, P. 695.

21 K. Miyamoto, M. Hanada, T. Inoue, N. Miyamoto, A. Nagase, Y. Ohara, Y. Okumura and K. Watanabe, *Proc. of the 18th Symposium on Fusion Technology, Karlsruher, 1994*, to be published.

22 Y. Takeiri, A. Ando, O. Kaneko, Y. Oka, K. Tsumori, R. Akiyama, E. Asano, T. Kawamoto, M. Tanaka and T. Kuroda, to be published in J. Plasma and Fusion Research **71**, No.7 (1995).

23 A. Iiyoshi, *Proc. of the 13th Symp. on Fusion Engineering, Knoxville, 1989*, p. 1007.

24 A. Iiyoshi, M. Fujiwara, O. Motojima, N. Ohyabu and K. Yamazaki, Fusion Technology **17**, 169 (1990).

25 Y. Takeiri, O. Kaneko, F. Sano, A. Ando, Y. Oka, K. Hanatani, T. Obiki and T. Kuroda, *Proc. of the first Int. Toki Conf. on Plasma Physics and Controlled Nuclear Fusion, Toki, Japan, 1989*, p. 272.

26 L. D. Stewart, J. Kim and S. Matsuda, Rev. Sci. Instrum. **46**, 1193 (1975)

27 J. R. Coupland and T. S. Green, Nucl. Instrum. Meth. **125**, 197 (1975).

28 W. L. Gardner, J. Kim, M. M. Menon and J. H. Whealton, Rev. Sci. Instrum. **49**, 1214 (1978).

29 J. R. Conrad, Rev. Sci. Instrum. **51**, 418 (1980).

30 Y. Okumura, Y. Mizutani and Y. Ohara, Rev. Sci. Instrum, **51**, 471 (1980).

31 T. Inoue, M. Hanada, M. Mizuno, Y. Ohara, Y. Okumura, Y. Suzuki, M. Tanaka and K. Watanabe, *Proc. of the 6th Int. Symp. on Production and Neutralization of Negative Ions and Beams, Upton, NY, 1992*, AIP Conf. Proc. No. 287, p. 316.

32 Y. Oka, A. Ando, O. Kaneko, Y. Takeiri, K. Tsumori, R. Akiyama, T. Kawamoto, K. Mineo, T. Kurata and T. Kuroda, *Proc. of the 14th Symp. on Fusion Engineering, San Diego, 1991*, p. 70.

33 O. Kaneko, A. Ando, Y. Oka, Y. Takeiri, K. Tsumori, R. Akiyama, T. Kawamoto, T. Kurata, K. Mineo and T. Kuroda, *Proc. of the 17th Symp.on Fusion Technology, Rome, 1992*, p. 544.

34 Y. Takeiri, A. Ando, O. Kaneko, Y. Oka, K. Tsumori, R. Akiyama, T. Kawamoto and T. Kuroda, *Proc. of the 6th Int. Symp. on Production and Neutralization of Negative Ions and Beams, Upton, NY, 1992*, AIP Conf. Proc. No. 287, p. 869.

35 Y. Takeiri, Y. Oka, O. Kaneko, A. Ando, K. Tsumori, R. Akiyama, T. Kawamoto and T. Kuroda, Rev. Sci. Instrum, **65**, 1198 (1994).

FIGURE CAPTIONS

Fig. 1 Schematic diagram of an external-filter-type large negative-ion source with a two-stage accelerator.

Fig. 2 Grid arrangements along the beam axis and the electrical connections of the power supplies in (a) the two-stage accelerator and (b) the single-stage accelerator. δ is the amount of the displacement and θ the steering angle. S and N denote the polarities of the permanent magnets.

Fig. 3 (a) and (b) vertical (Y) profiles measured by the calorimeter arrays located 5 m and 11.2 m downstream from the ion source, respectively, and (c) and (d) the horizontal (X) profiles measured 5 m and 11.2 m downstream, respectively, in the two-stage acceleration. The total beam energy is 111 keV, the total H^- ion current 5 m downstream 3.8 A and the second acceleration voltage 72 kV. The dotted lines show calculated beam profiles using multi-gaussian beamlets with the divergence angle of 9 mrad and the alternate horizontal deflection angle of ± 8 mrad.

Fig. 4 (a) FWHMs of the vertical profiles measured 5 m (●) and 11.2 m (○) downstream from the ion source, and (b) the H^- ion current (●) and the ratio of the H^- ion current to the second acceleration current, I_{H^-}/I_{acc2} (○), as a function of the ratio of the first acceleration to the extraction electric fields, E_{acc1}/E_{ext}, in the two-stage acceleration. The arc power is 70 kW and the extraction voltage is 6.2 kV. The ratio of the first to the second acceleration electric fields, E_{acc1}/E_{acc2}, is constant, 0.93.

Fig. 5 e-folding half width of the vertical profile measured 11.2 m

downstream from the ion source as a function of the ratio of the first acceleration to the extraction electric fields, E_{accl}/E_{ext}, in the two-stage acceleration on the same conditions as those in Fig. 4. The corresponding gross divergence angle estimated from the e-folding half width is also indicated on the right hand axis.

Fig. 6 (a) and (b) vertical (Y) profiles measured 5 m and 11.2 m downstream from the ion source, respectively, and (c) and (d) the horizontal (X) profiles measured 5 m and 11.2 m downstream, respectively, in the single-stage acceleration. The total beam energy is 83 keV, the total H^- ion current 5 m downstream 3.8 A and the acceleration voltage 78 kV. The dotted lines show calculated beam profiles using multi-gaussian beamlets with the divergence angle of 9 mrad and the alternate horizontal deflection angle of ± 2 mrad.

Fig. 7 (a) e-folding half width of the vertical profiles 11.2 m downstream and (b) the total H^- ion currents measured 11.2 m downstream, in the single-stage acceleration as a function of the acceleration voltage for the extraction voltages of 5.2 (●), 4.3 (○) and 3.4 (△) kV. The gross divergence angle corresponding to the e-folding half width is also indicated on the right hand axis in (a). The arc power is 60 kW.

Fig. 8 (a) e-folding half width of the vertical profiles and (b) the total H^- ion current both measured 11.2 m downstream in the single-stage acceleration, as a function of the ratio of the acceleration to the extraction electric fields, E_{acc}/E_{ext}, for the extraction voltages, V_{ext}, of 5.2 (▲), 4.3 (○) and 3.4 (□) kV at the arc power, P_{arc}, of 60

kW and the V_{ext} of 4.4 ($\triangledown$) and 3.6 ($\triangle$) kV at the P_{arc} of 35 kW. The divergence angle corresponding to the e-folding half width is also indicated on the right hand axis in (a).

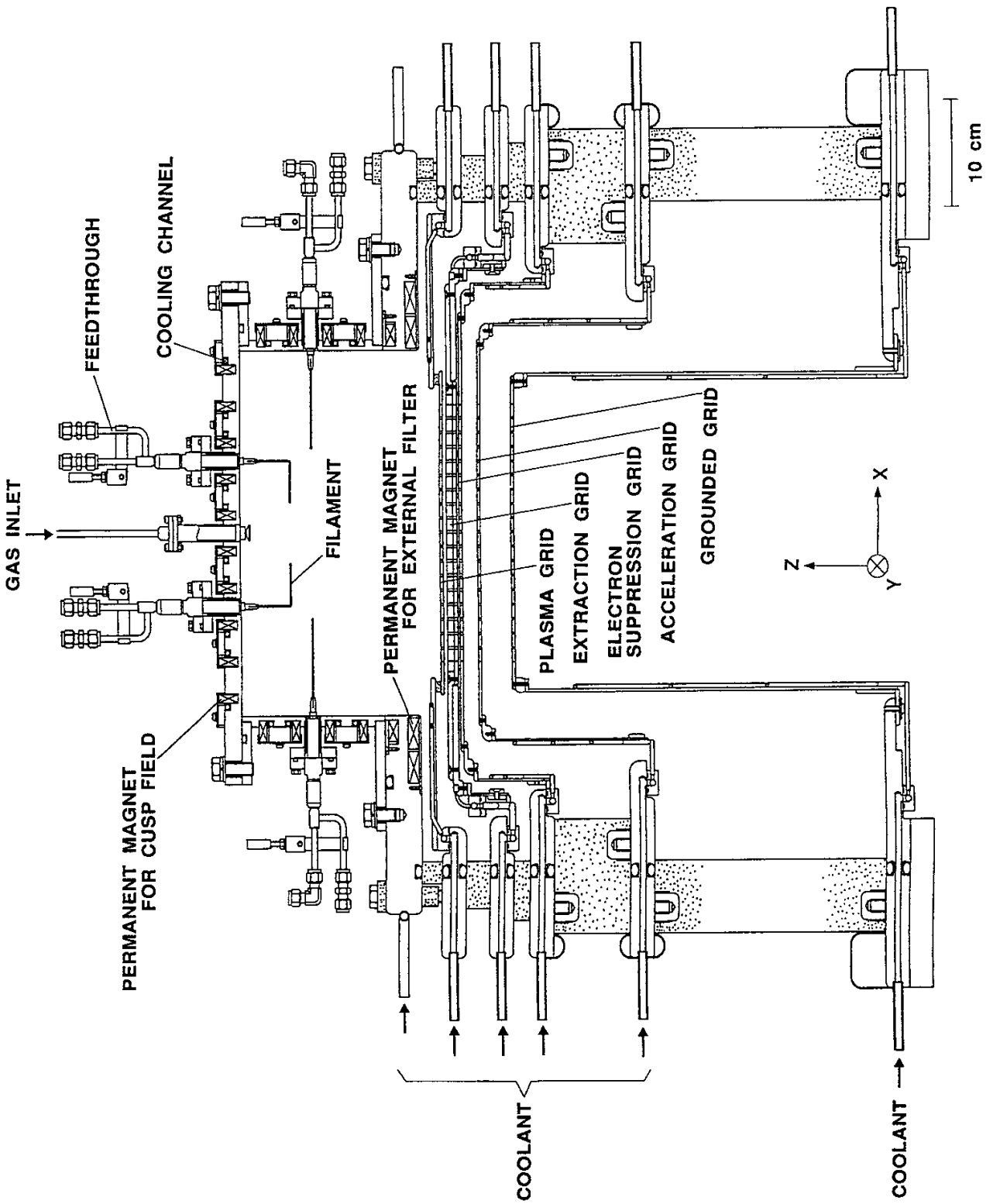

Figure 1
Y. Takeiri, *et al.*

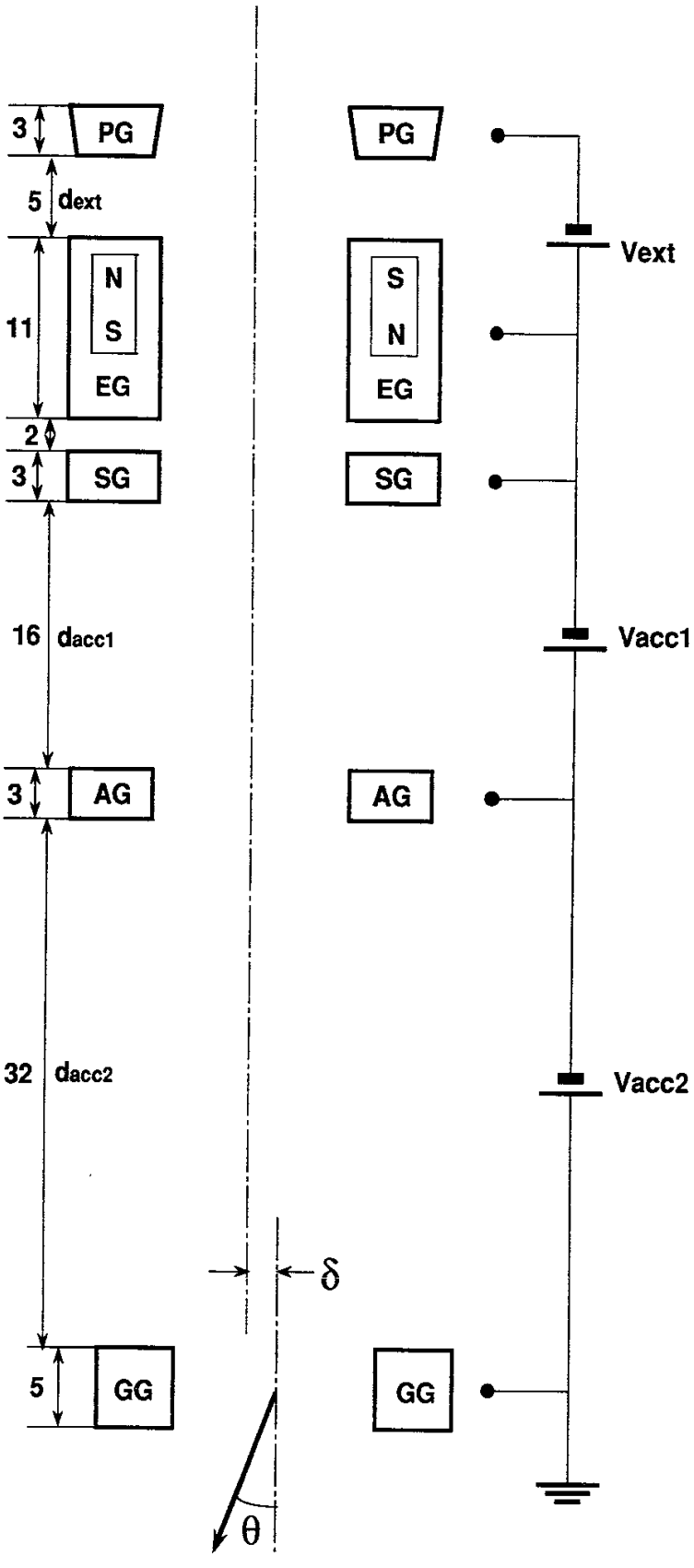

(a)

Figure 2 (a)
Y. Takeiri, *et al.*

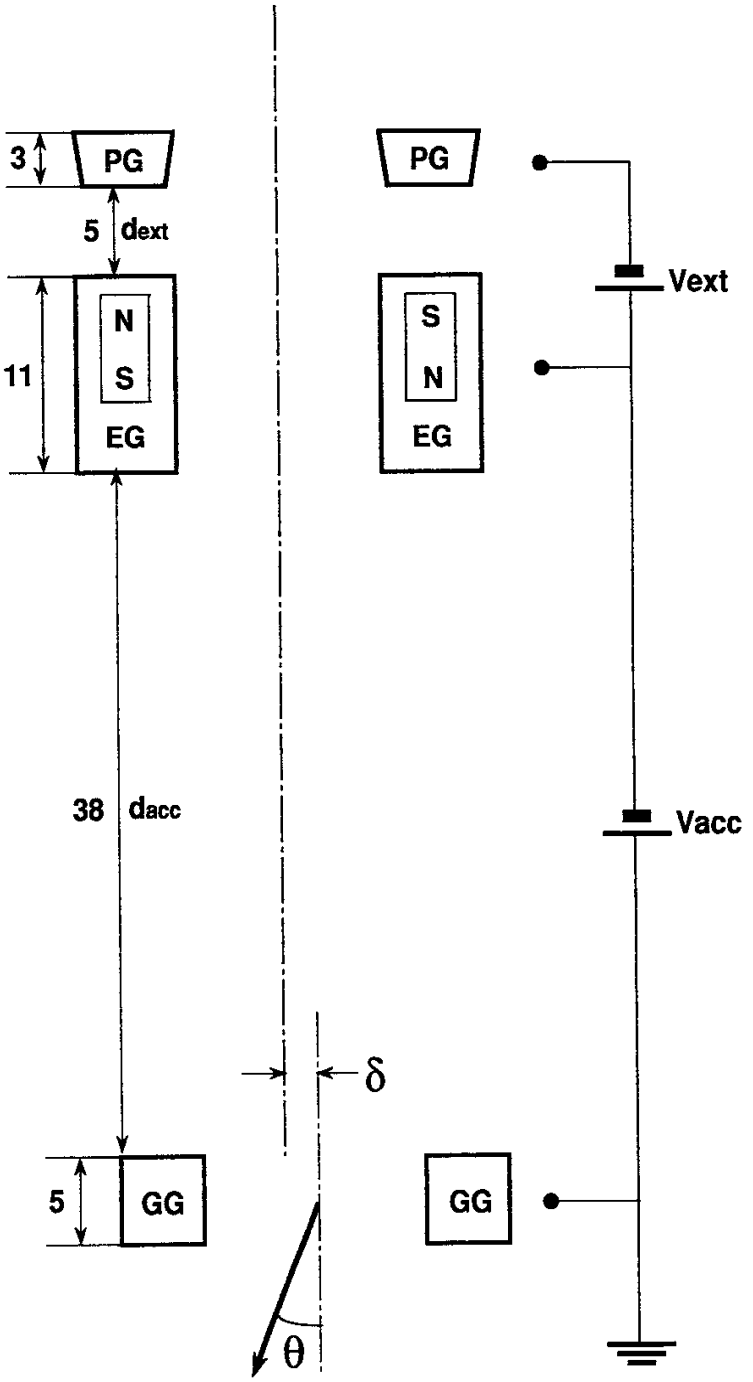

(b)

Figure 2 (b)
Y. Takeiri, *et al.*

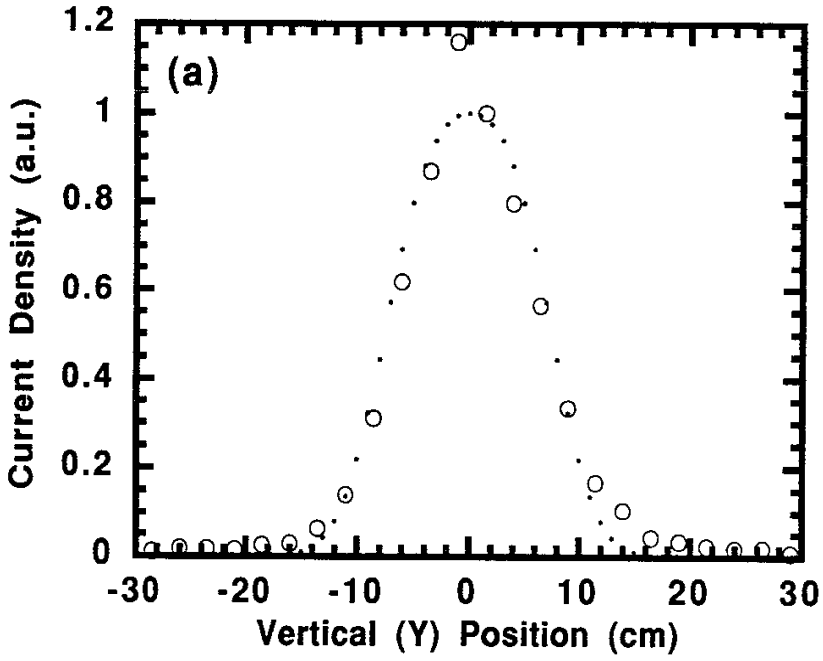

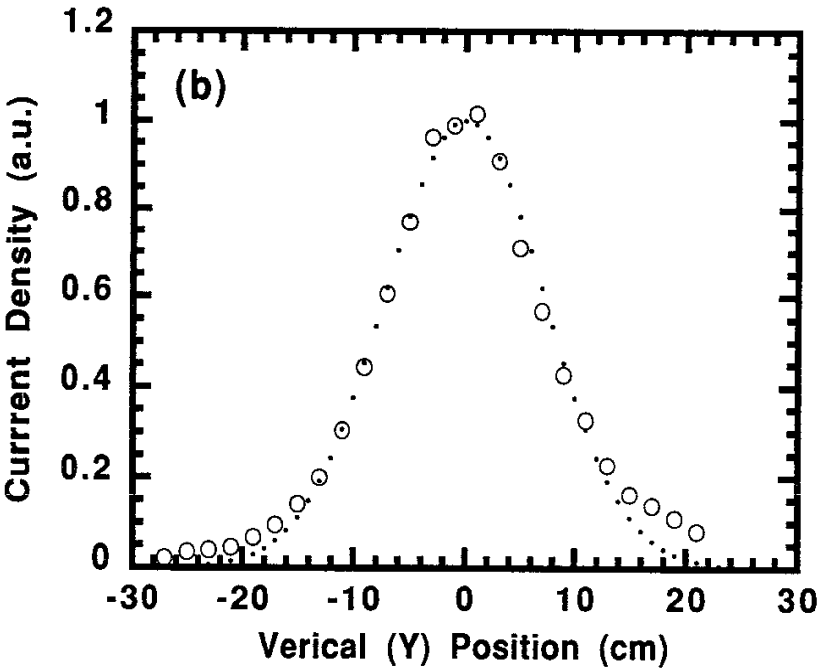

Figures 3 (a) and (b)
Y. Takeiri, *et al.*

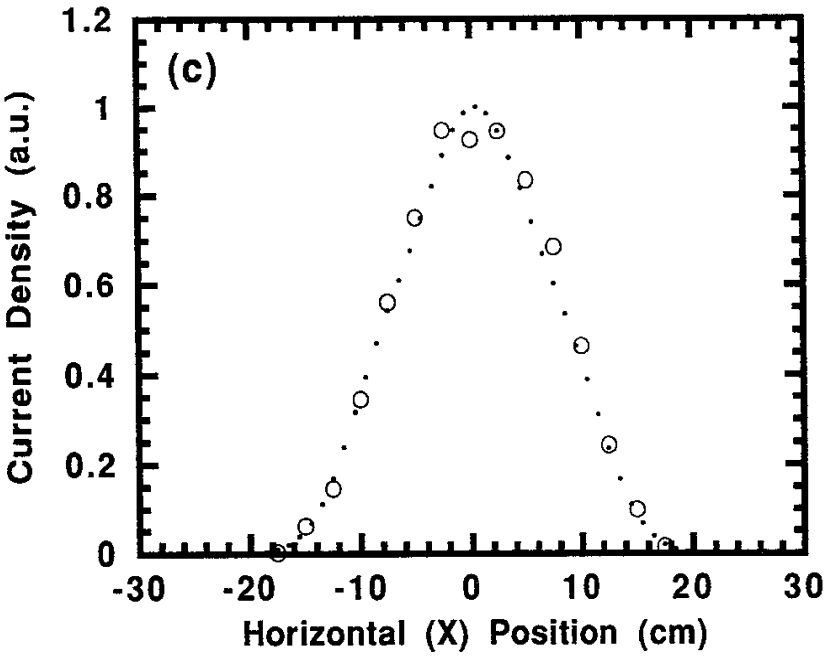

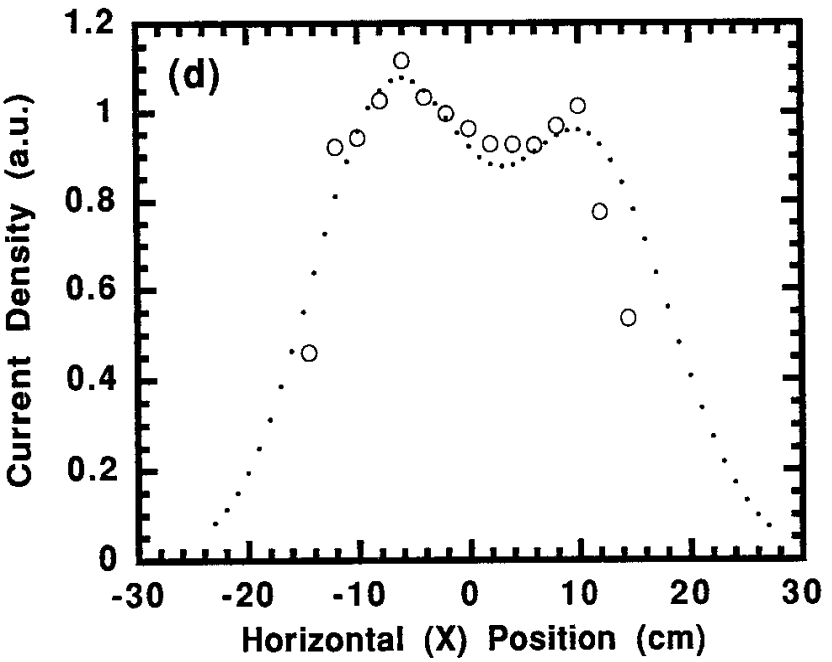

Figures 3 (c) and (d)
Y. Takeiri, *et al.*

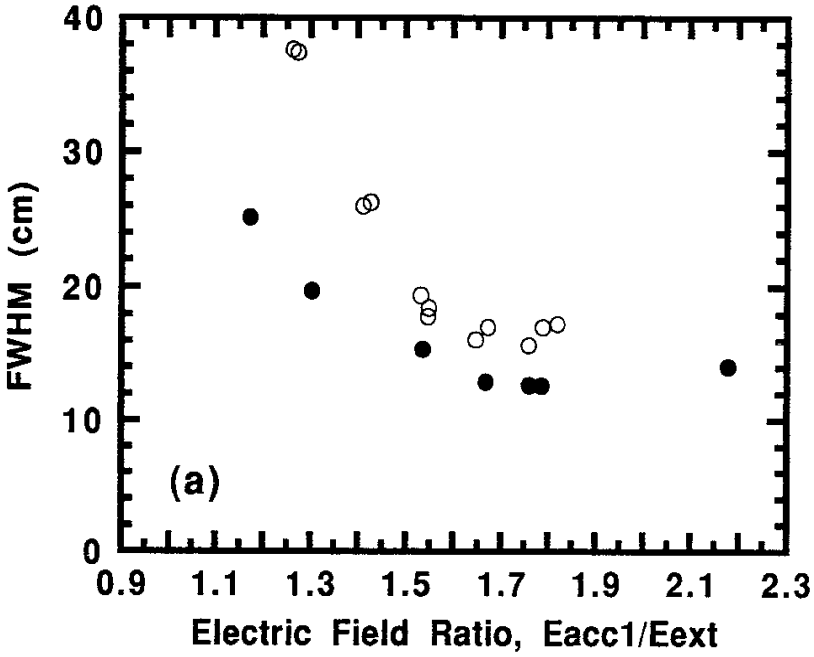

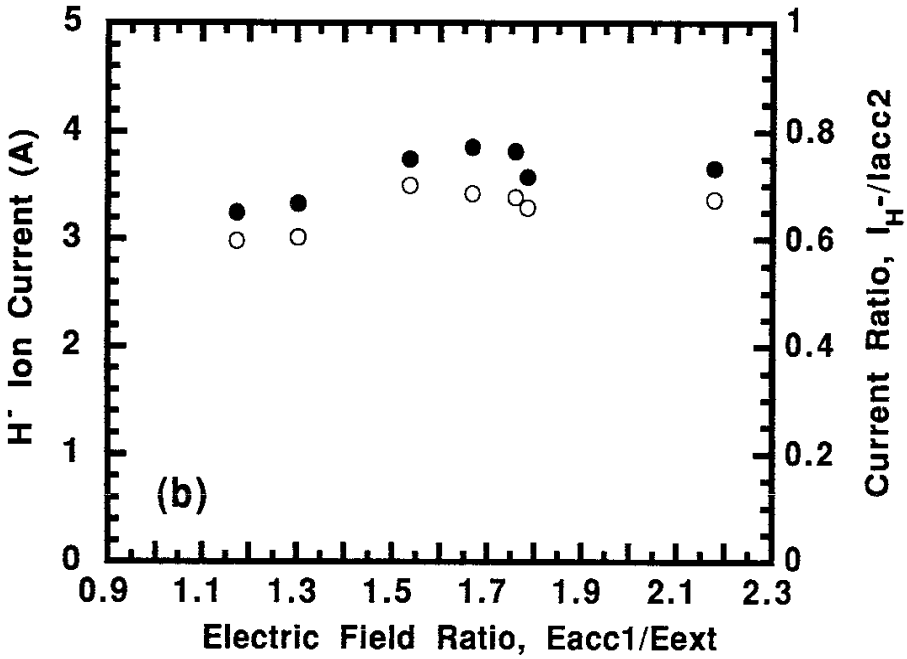

Figure 4
Y. Takeiri, *et al.*

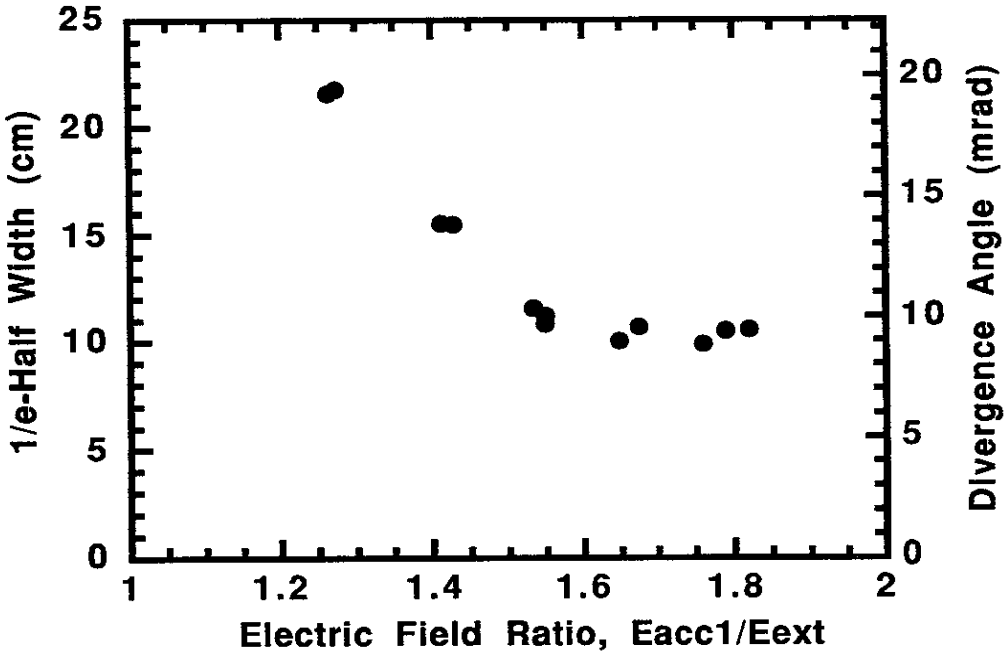

Figure 5
Y. Takeiri, *et al.*

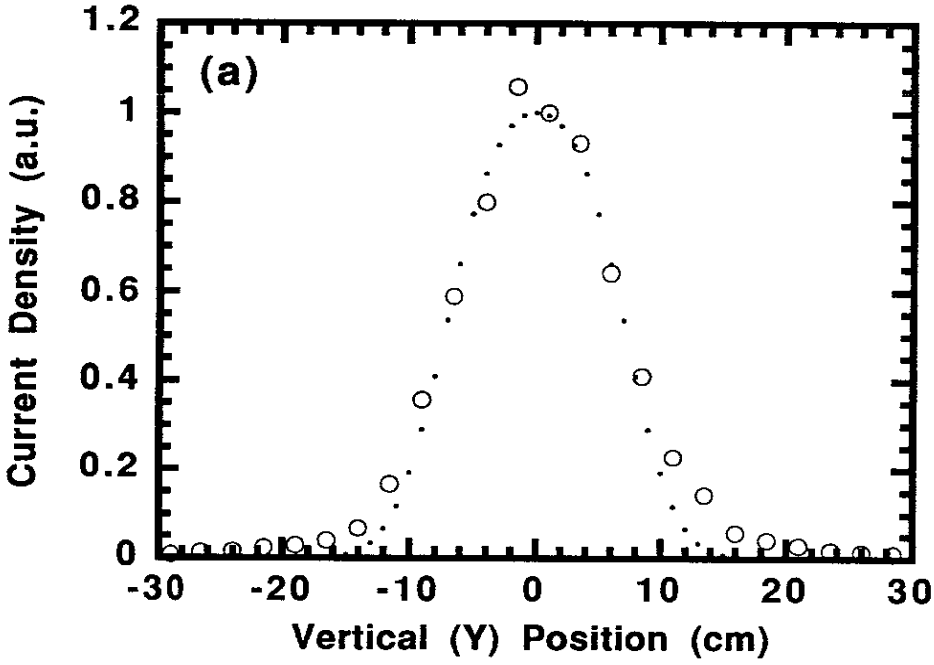

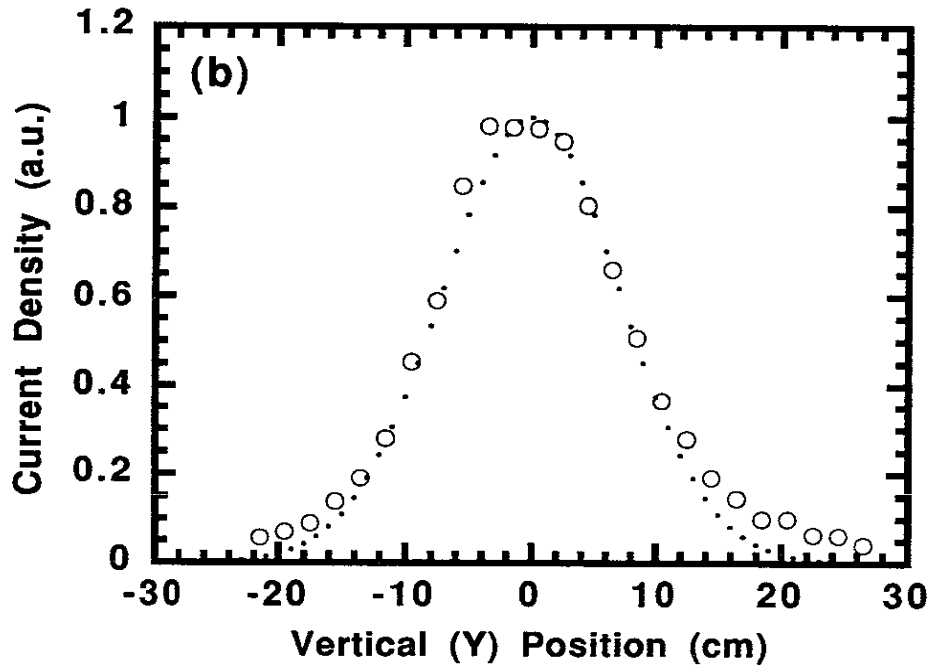

Figures 6 (a) and (b)
Y. Takeiri, *et al.*

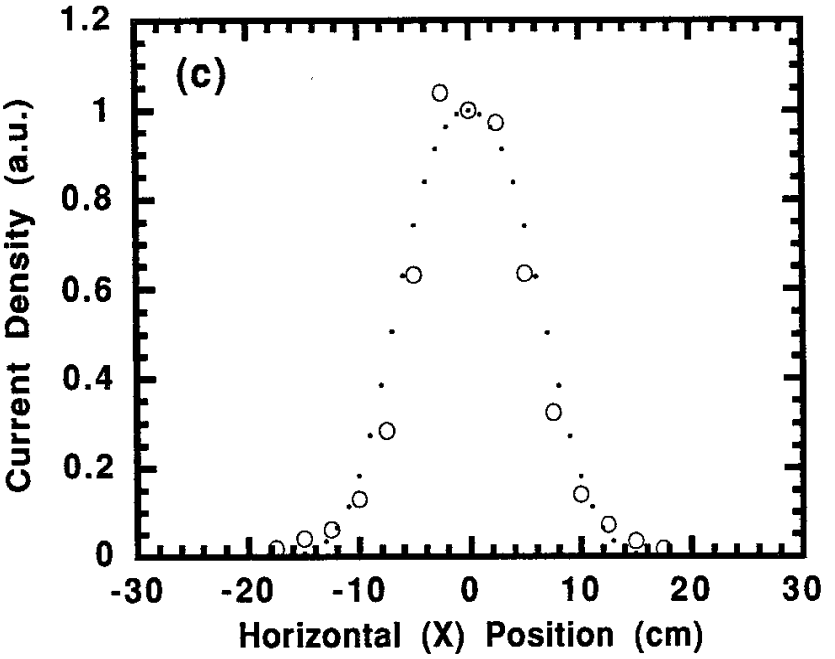

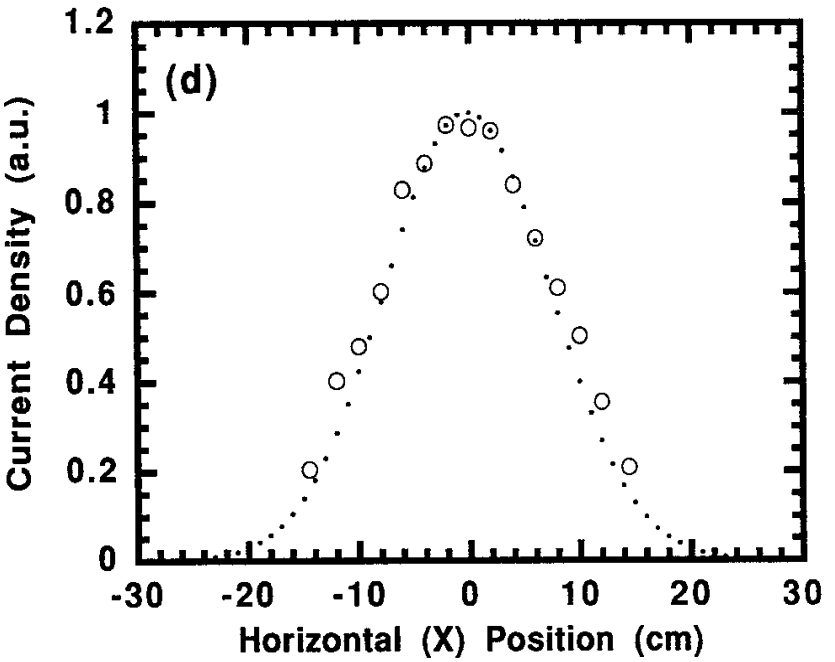

Figures 6 (c) and (d)
Y. Takeiri, *et al.*

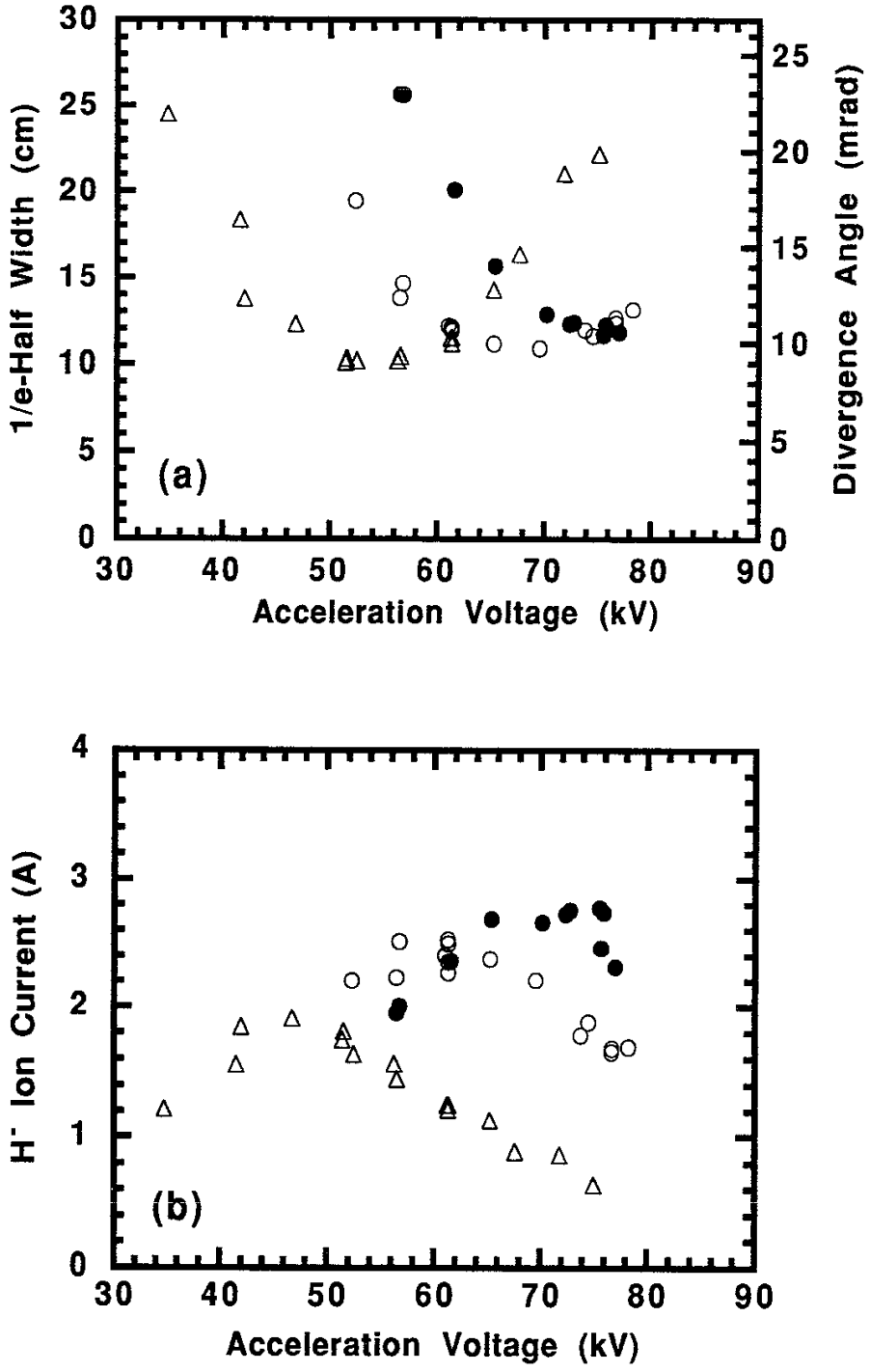

Figure 7
Y. Takeiri, *et al.*

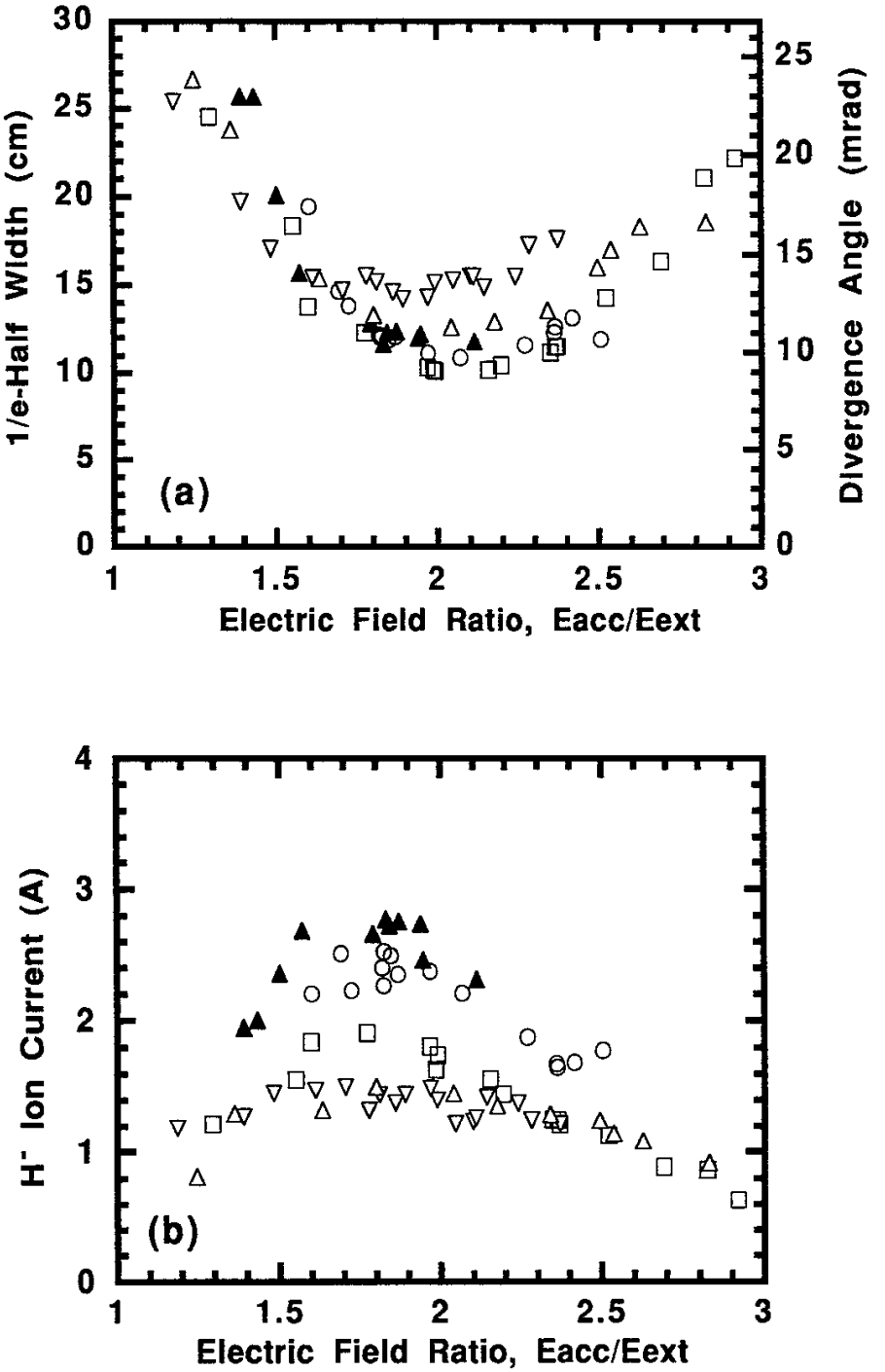

Figure 8
Y. Takeiri, *et al.*

Recent Issues of NIFS Series

NIFS-318 T. Sato and Complexity Simulation Group,
Complexity in Plasma - A Grand View of Self- Organization; Nov. 1994

NIFS-319 Y. Todo, T. Sato, K. Watanabe, T.H. Watanabe and R. Horiuchi,
MHD-Vlasov Simulation of the Toroidal Alfvén Eigenmode; Nov. 1994

NIFS-320 A. Kageyama, T. Sato and The Complexity Simulation Group,
Computer Simulation of a Magnetohydrodynamic Dynamo II: Nov. 1994

NIFS-321 A. Bhattacharjee, T. Hayashi, C.C.Hegna, N. Nakajima and T. Sato,
Theory of Pressure-induced Islands and Self-healing in Three-dimensional Toroidal Magnetohydrodynamic Equilibria; Nov. 1994

NIFS-322 A. Iiyoshi, K. Yamazaki and the LHD Group,
Recent Studies of the Large Helical Device: Nov. 1994

NIFS-323 A. Iiyoshi and K. Yamazaki,
The Next Large Helical Devices; Nov. 1994

NIFS-324 V.D. Pustovitov
Quasisymmetry Equations for Conventional Stellarators; Nov. 1994

NIFS-325 A. Taniike, M. Sasao, Y. Hamada, J. Fujita, M. Wada,
The Energy Broadening Resulting from Electron Stripping Process of a Low Energy Au^- Beam; Dec. 1994

NIFS-326 I. Viniar and S. Sudo,
New Pellet Production and Acceleration Technologies for High Speed Pellet Injection System "HIPEL" in Large Helical Device; Dec. 1994

NIFS-327 Y. Hamada, A. Nishizawa, Y. Kawasumi, K. Kawahata, K. Itoh, A. Ejiri, K. Toi, K. Narihara, K. Sato, T. Seki, H. Iguchi, A. Fujisawa, K. Adachi, S. Hidekuma, S. Hirokura, K. Ida, M. Kojima, J. Koong, R. Kumazawa, H. Kuramoto, R. Liang, T. Minami, H. Sakakita, M. Sasao, K.N. Sato, T. Tsuzuki, J. Xu, I. Yamada, T. Watari,
Fast Potential Change in Sawteeth in JIPP T-IIU Tokamak Plasmas; Dec. 1994

NIFS-328 V.D. Pustovitov,
Effect of Satellite Helical Harmonics on the Stellarator Configuration; Dec. 1994

NIFS-329 K. Itoh, S-I. Itoh and A. Fukuyama,
A Model of Sawtooth Based on the Transport Catastrophe; Dec. 1994

NIFS-330 K. Nagasaki, A. Ejiri,
Launching Conditions for Electron Cyclotron Heating in a Sheared

Magnetic Field; Jan. 1995

NIFS-331 T.H. Watanabe, Y. Todo, R. Horiuchi, K. Watanabe, T. Sato,
An Advanced Electrostatic Particle Simulation Algorithm for Implicit Time Integration; Jan. 1995

NIFS-332 N. Bekki and T. Karakisawa,
Bifurcations from Periodic Solution in a Simplified Model of Two-dimensional Magnetoconvection; Jan. 1995

NIFS-333 K. Itoh, S.-I. Itoh, M. Yagi, A. Fukuyama,
Theory of Anomalous Transport in Reverse Field Pinch; Jan. 1995

NIFS-334 K. Nagasaki, A. Isayama and A. Ejiri
Application of Grating Polarizer to 106.4GHz ECH System on Heliotron-E; Jan. 1995

NIFS-335 H. Takamaru, T. Sato, R. Horiuchi, K. Watanabe and Complexity Simulation Group,
A Self-Consistent Open Boundary Model for Particle Simulation in Plasmas; Feb. 1995

NIFS-336 B.B. Kadomtsev,
Quantum Telegragh : is it possible?; Feb. 1995

NIFS-337 B.B.Kadomtsev,
Ball Lightning as Self-Organization Phenomenon; Feb. 1995

NIFS-338 Y. Takeiri, A. Ando, O. Kaneko, Y. Oka, K. Tsumori, R. Akiyama, E. Asano, T. Kawamoto, M. Tanaka and T. Kuroda,
High-Energy Acceleration of an Intense Negative Ion Beam; Feb. 1995

NIFS-339 K. Toi, T. Morisaki, S. Sakakibara, S. Ohdachi. T.Minami, S. Morita, H. Yamada, K. Tanaka, K. Ida, S. Okamura, A. Ejiri, H. Iguchi, K. Nishimura, K. Matsuoka, A. Ando, J. Xu, I. Yamada, K. Narihara, R. Akiyama, H. Idei, S. Kubo, T. Ozaki, C. Takahashi, K. Tsumori,
H-Mode Study in CHS; Feb. 1995

NIFS-340 T. Okada and H. Tazawa,
Filamentation Instability in a Light Ion Beam-plasma System with External Magnetic Field; Feb. 1995

NIFS-341 T. Watanbe, G. Gnudi,
A New Algorithm for Differential-Algebraic Equations Based on HIDM; Feb. 13, 1995

NIFS-342 Y. Nejoh,
New Stationary Solutions of the Nonlinear Drift Wave Equation; Feb. 1995

NIFS-343 A. Ejiri, S. Sakakibara and K. Kawahata,
Signal Based Mixing Analysis for the Magnetohydrodynamic Mode Reconstruction from Homodyne Microwave Reflectometry; Mar.. 1995

NIFS-344 B.B.Kadomtsev, K. Itoh, S.-I. Itoh
Fast Change in Core Transport after L-H Transition; Mar. 1995

NIFS-345 W.X. Wang, M. Okamoto, N. Nakajima and S. Murakami,
An Accurate Nonlinear Monte Carlo Collision Operator; Mar. 1995

NIFS-346 S. Sasaki, S. Takamura, S. Masuzaki, S. Watanabe, T. Kato, K. Kadota,
Helium I Line Intensity Ratios in a Plasma for the Diagnostics of Fusion Edge Plasmas; Mar. 1995

NIFS-347 M. Osakabe,
Measurement of Neutron Energy on D-T Fusion Plasma Experiments; Apr. 1995

NIFS-348 M. Sita Janaki, M.R. Gupta and Brahmananda Dasgupta,
Adiabatic Electron Acceleration in a Cnoidal Wave; Apr. 1995

NIFS-349 J. Xu, K. Ida and J. Fujita,
A Note for Pitch Angle Measurement of Magnetic Field in a Toroidal Plasma Using Motional Stark Effect; Apr. 1995

NIFS-350 J. Uramoto,
Characteristics for Metal Plate Penetration of a Low Energy Negative Muonlike or Pionlike Particle Beam: Apr. 1995

NIFS-351 J. Uramoto,
An Estimation of Life Time for A Low Energy Negative Pionlike Particle Beam: Apr. 1995

NIFS-352 A. Taniike,
Energy Loss Mechanism of a Gold Ion Beam on a Tandem Acceleration System: May 1995

NIFS-353 A. Nishizawa, Y. Hamada, Y. Kawasumi and H. Iguchi,
Increase of Lifetime of Thallium Zeolite Ion Source for Single-Ended Accelerator: May 1995

NIFS-354 S. Murakami, N. Nakajima, S. Okamura and M. Okamoto,
Orbital Aspects of Reachable β Value in NBI Heated Heliotron/Torsatrons; May 1995

NIFS-355 H. Sugama and W. Horton,
Neoclassical and Anomalous Transport in Axisymmetric Toroidal Plasmas with Electrostatic Turbulence; May 1995

NIFS-356 N. Ohyabu
A New Boundary Control Scheme for Simultaneous Achievement of H-mode and Radiative Cooling (SHC Boundary); May 1995

NIFS-357 Y. Hamada, K.N. Sato, H. Sakakita, A. Nishizawa, Y. Kawasumi, R. Liang, K. Kawahata, A. Ejiri, K. Toi, K. Narihara, K. Sato, T. Seki, H. Iguchi, A. Fujisawa, K. Adachi, S. Hidekuma, S. Hirokura, K. Ida, M. Kojima, J. Koong, R. Kumazawa, H. Kuramoto, T. Minami,. M. Sasao, T. Tsuzuki, J.Xu, I. Yamada, and T. Watari,
Large Potential Change Induced by Pellet Injection in JIPP T-IIU Tokamak Plasmas; May 1995

NIFS-358 M. Ida and T. Yabe,
Implicit CIP (Cubic-Interpolated Propagation) Method in One Dimension; May 1995

NIFS-359 A. Kageyama, T. Sato and The Complexity Simulation Group,
Computer Has Solved A Historical Puzzle: Generation of Earth's Dipole Field; June 1995

NIFS-360 K. Itoh, S.-I. Itoh, M. Yagi and A. Fukuyama,
Dynamic Structure in Self-Sustained Turbulence; June 1995

NIFS-361 K. Kamada, H. Kinoshita and H. Takahashi,
Anomalous Heat Evolution of Deuteron Implanted Al on Electron Bombardment; June 1995

NIFS-362 V.D. Pustovitov,
Suppression of Pfirsch-schlüter Current by Vertical Magnetic Field in Stellarators; June 1995

NIFS-363 A. Ida, H. Sanuki and J. Todoroki
An Extended K-dV Equation for Nonlinear Magnetosonic Wave in a Multi-Ion Plasma; June 1995

NIFS-364 H. Sugama and W. Horton
Entropy Production and Onsager Symmetry in Neoclassical Transport Processes of Toroidal Plasmas; July 1995

NIFS-365 K. Itoh, S.-I. Itoh, A. Fukuyama and M. Yagi,
On the Minimum Circulating Power of Steady State Tokamaks; July 1995

NIFS-366 K. Itoh and Sanae-I. Itoh,
The Role of Electric Field in Confinement; July 1995

NIFS-367 F. Xiao and T. Yabe
A Rational Function Based Scheme for Solving Advection Equation; July 1995